Transactions, **SMiRT-26**
Berlin/Potsdam, Germany, July 10-15, 2022
Division VIII

NON-CONTACT DETECTION OF THE ADHESIVE PROPERTIES OF CERAMIC COATINGS FOR HIGH TEMPERATURE APPLICATIONS USING INFRARED THERMOGRAPHY

Jochen Manara[1], Thomas Stark[2], Mariacarla Arduini[3], Hans-Peter Ebert[4], Kevin Knopp[5], Amir Shandy[6] and Jürgen Hartmann[7]

[1]Dr., Bavarian Center for Applied Energy Research (ZAE Bayern), Würzburg, Germany (jochen.manara@zae-bayern.de)
[2]Physicist, Bavarian Center for Applied Energy Research (ZAE Bayern), Würzburg, Germany
[3]Engineer, Bavarian Center for Applied Energy Research (ZAE Bayern), Würzburg, Germany
[4]Dr., Bavarian Center for Applied Energy Research (ZAE Bayern), Würzburg, Germany
[5]Doctoral Student, University of Applied Sciences Würzburg-Schweinfurt (FHWS), Schweinfurt, Germany
[6]Doctoral Student, University of Applied Sciences Würzburg-Schweinfurt (FHWS), Schweinfurt, Germany
[7]Prof. Dr., University of Applied Sciences Würzburg-Schweinfurt (FHWS), Schweinfurt, Germany and Bavarian Center for Applied Energy Research (ZAE Bayern), Würzburg, Germany

ABSTRACT

Industries such as glass, nuclear, space and aeronautics continuously need to design new products and improve the existing ones in order to remain competitive in their market. Additionally the mechanical properties need to be determined and non-destructive examination (NDE) methods are preferable for testing structural integrity of the applied materials, including protective coatings. Hence, the focus of this work lies on the development of non-destructive and contactless methods for determining the adhesive properties of ceramic coatings for high temperature applications during maintenance as well as during operation. The adhesive properties of layer systems are closely correlated with the thermal contact resistance of these layers. Both, large-area reduction and small-area reduction of the mechanical adhesion may lead to a local delamination of the coating, which degrades the properties of the system including a total failure of the system.

Therefore, a non-contact measurement technique has been developed in this work, which is based on a thermographic device. For inspecting the surface, the investigated object is thermally excited with a suitable non-contact heating method (e.g. laser-heating) and the resulting temperature distribution on the surface is recorded using a thermographic camera. Since an existing delamination increases the thermal contact resistance between the coating and the substrate, the heat transfer from the coating to the underlying substrate is locally reduced, which results in a locally higher temperature.

For optimal evaluation of the measurement results and the derived temperature distributions, the infrared-optical properties of the ceramic coatings (especially spectral emittance and transmittance) as well as of the metal substrates (spectral emittance and reflectance) are also required. These values were measured on specially prepared samples as a function of temperature. Due to the consideration of partially transparent and non-transparent spectral ranges of the ceramic coatings, radiation can penetrate the coatings to different depths or radiation is detected from different depths, which must be taken into account in each case during the evaluation.

INTRODUCTION

Protective layers and thermal barrier coatings based on ceramic materials are used in various applications (e.g. in stationary gas turbines and jet engines or in nuclear and fusion reactors) to protect the underlying metallic substrate from harsh environments. Besides the optical and thermal properties of the ceramic coatings, such as emittance and thermal conductivity, the structural integrity or more specifically the mechanical properties, mainly the adhesion of the coating to the substrate, are of great importance.

A major failure mechanism is the formation of an oxide layer between the metallic substrate and the ceramic coating [Nitin et al. (2002)]. Specifically, this is a thermally grown oxide (TGO) layer, which is formed at high temperatures upon the substrate or bond coat due to the diffusion of oxygen through the ceramic layer. This mechanism is illustrated in Figure 1 for typical ceramic-based top-coats, which are prepared by either electron beam physical vapor deposition (EB-PVD on the left) or atmospheric plasma spraying (APS on the right) on NiCrAlY-based bond coats. As the thickness of the TGO layer increases, the risk of delamination of the top-coat increases. Other failure mechanisms, which may also lead to a debonding of the ceramic coating are thermal shock [Zhang et al. (2019)] and sintering effects of the ceramic material [Ahrens et al. (2004)]. Usually, local delamination occurs first as a precursor to large-scale debonding and finally to complete layer failure, which may lead to considerable damage during operation. A number of other theoretical studies have been carried out to explain the delamination of coating systems [Choi et al. (199), Evans et al. (2001), Hutchinson and Evans (2002)]. However, up to now there has been a lack of comprehensive and meaningful experimental studies on the adhesion and debonding of coatings for substantiating these theoretical models experimentally on real coatings.

Current inspection methods are predominantly based either on destructive testing (e.g. sawing and inspecting the cross-section) or require contact sensors (e.g. ultrasonic testing) that must be applied to the surface. Besides, there are also approaches to apply non-destructive methods. In this context, methods based on eddy current technology [Li et al. (2012)], TGO luminescence [Tolpygo et al. (2004)] and laser-based acoustic emission [Ito et al. (2014)] have been used. In addition, the use of thermographic devices is described in literature [Eldridge et al. (2006)]. However, these methods need complex instrumentation and measurements were often performed over a relatively wide, non-customized spectral range. Hence, a still existing key issue is therefore the non-destructive and contactless detection of local delaminations during operation at high temperatures or at service intervals with optimized equipment and customized spectral ranges.

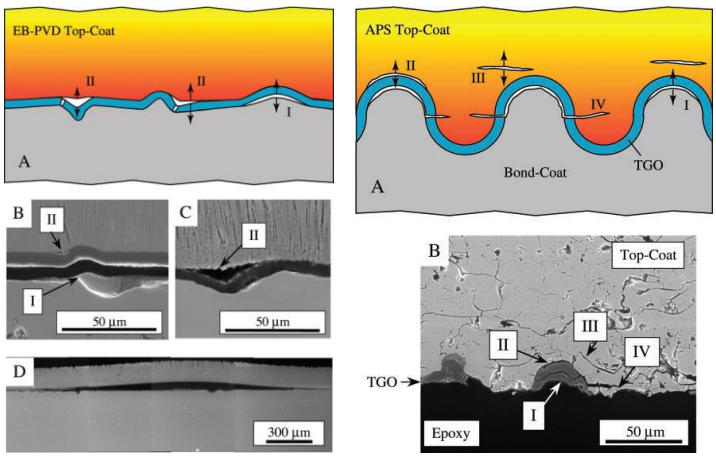

Figure 1. Scanning electron microscope images and schematic illustrations of possible delamination mechanisms of coatings prepared by electron beam physical vapor deposition (EB-PVD on the left) and atmospheric plasma spraying (APS on the right). The illustrations are taken from Nitin et al. (2002).

INFRARED-OPTICAL CHARACTERIZATION

For performing non-destructive and contactless examinations using thermographic devices or radiation thermometers, the knowledge of the optical and infrared-optical properties of the investigated materials and coatings are necessary. Hence, two spectrometric setups have been used for performing measurements at ambient and high temperatures, which are explained below.

At ambient temperature, a FTIR-spectrometer with an integrating sphere setup [Hanssen (2001)] has been used for measuring the spectral directional-hemispherical reflectance $R_{\mathrm{dh},\lambda}$ and transmittance $T_{\mathrm{dh},\lambda}$ (Figure 2). The spectral directional emittance $\varepsilon_{\mathrm{d},\lambda}$ can then be calculated from the derived spectral directional-hemispherical reflectance $R_{\mathrm{dh},\lambda}$ and transmittance $T_{\mathrm{dh},\lambda}$ by [Manara et al. (2009a)]

$$\varepsilon_{\mathrm{d},\lambda} = 1 - R_{\mathrm{dh},\lambda} - T_{\mathrm{dh},\lambda} \quad . \tag{1}$$

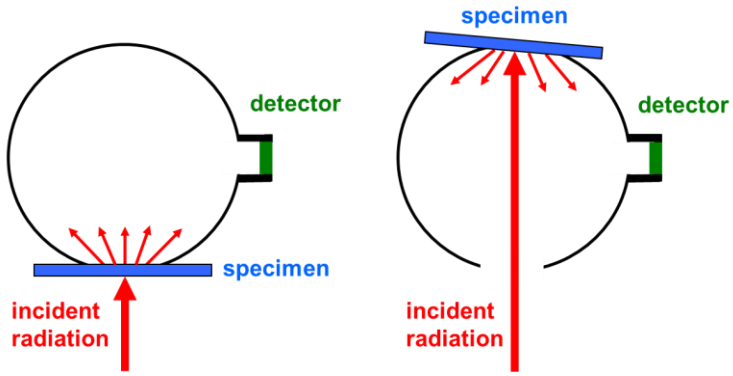

Figure 2. Measurement of the spectral directional-hemispherical transmittance $T_{\mathrm{dh},\lambda}$ (on the left) and the spectral directional-hemispherical reflectance $R_{\mathrm{dh},\lambda}$ (on the right) using an integrating sphere.

At first, typical ceramic materials have been investigated at ZAE Bayern, which are used for protective coatings, such as alumina (Al_2O_3). For the experimental characterization, free-standing slices with different thicknesses *d* have been prepared. The resulting spectra of alumina with a porosity of 2 % are depicted in Figure 3 at ambient temperature.

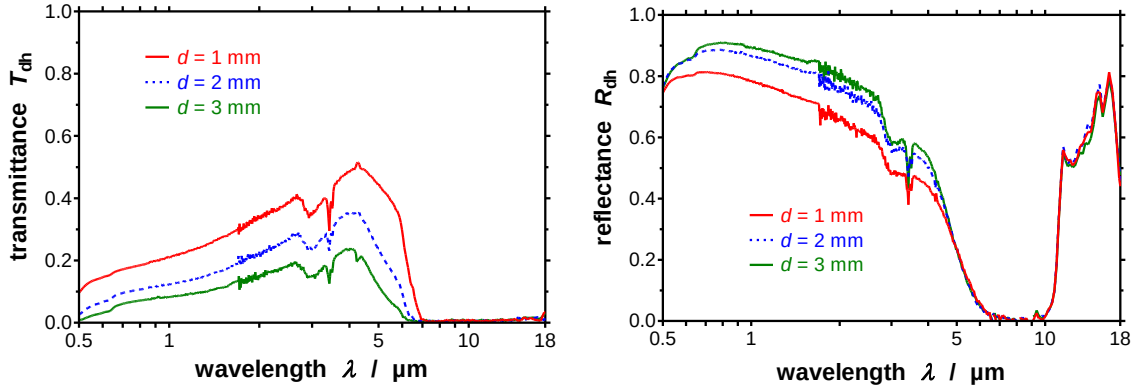

Figure 3. Directional-hemispherical transmittance $T_{\mathrm{dh},\lambda}$ (left graph) and reflectance $R_{\mathrm{dh},\lambda}$ (right graph) of free-standing Al_2O_3-slices with different thicknesses *d*, but with identical structural properties and a porosity of 2 %, versus wavelength from 0.5 µm to 18 µm, at ambient temperature.

As most oxide ceramics, alumina is semi-transparent in the wavelength range up to about 7 µm, which has to be considered for non-contact temperature measurements. At higher wavelengths, the transmittance vanishes and the reflectance is low, which is correlated to a high emittance around 10 µm. For wavelengths above 12 µm the reflectance increases, which leads to the so-called Reststrahlen band.

For determining the infrared-optical properties at high temperatures, the black body boundary conditions (BBC) method has been used [Manara et al. (2001)]. With the BBC the spectral directional emittance $\varepsilon_{\mathrm{d},\lambda}$ and the spectral directional-hemispherical transmittance $T_{\mathrm{dh},\lambda}$ can be measured at high temperatures as well as the spectral directional-hemispherical reflectance $R_{\mathrm{dh},\lambda}$ [Manara et al. (2009b)]. The basic idea of the BBC is to obtain the optical properties of the sample at the temperature T_{sp} by varying the boundary conditions (Figure 4). As boundary condition for the front side and the back side of the sample a respective black enclosure is used. The boundary conditions can be varied by changing the temperatures of the black enclosures between the temperatures T_{b} and T_{a}. The sample is firstly heated in a furnace to the desired temperature T_{sp} with a homogenous temperature distribution inside. Afterwards the hot sample is quickly placed between the two black enclosures. For optimized measurements the temperature of the sample, T_{sp} is higher than the temperatures of the black enclosures T_{b} and T_{a}, whereat T_{b} is higher than T_{a}, i.e.

$$T_{\mathrm{sp}} > T_{\mathrm{b}} > T_{\mathrm{a}} \quad . \tag{2}$$

In Figure 4 (a) the sample at the temperature T_{sp} is surrounded by two black enclosures at the temperatures T_{b}. The detected intensity (long arrow) consists of three components:

- the spectral intensity, which is emitted from the sample at the temperature T_{sp}:
$$\varepsilon_{\mathrm{d},\lambda}(T_{\mathrm{sp}}) \cdot i_{\lambda,\mathrm{bb}}(T_{\mathrm{sp}}).$$
- the black body spectral intensity $i_{\lambda,\mathrm{bb}}$ from the rear side at the temperature T_{b}, which is transmitted through the sample:
$$T_{\mathrm{dh},\lambda}(T_{\mathrm{sp}}) \cdot i_{\lambda,\mathrm{bb}}(T_{\mathrm{b}}).$$
- the black body spectral intensity $i_{\lambda,\mathrm{bb}}$ from the front side at the temperature T_{b}, which is reflected by the sample:
$$R_{\mathrm{dh},\lambda}(T_{\mathrm{sp}}) \cdot i_{\lambda,\mathrm{bb}}(T_{\mathrm{b}}).$$

Thus the detected overall spectral intensity $i_{\lambda,\mathrm{meas}}$ is:

$$i_{\lambda,\mathrm{meas}}(T_{\mathrm{sp}}, T_{\mathrm{b}}) = \varepsilon_{\mathrm{d},\lambda}(T_{\mathrm{sp}}) \cdot i_{\lambda,\mathrm{bb}}(T_{\mathrm{sp}}) + \left[R_{\mathrm{dh},\lambda}(T_{\mathrm{sp}}) + T_{\mathrm{dh},\lambda}(T_{\mathrm{sp}})\right] \cdot i_{\lambda,\mathrm{bb}}(T_{\mathrm{b}}) \quad . \tag{3}$$

Equation (3) can be solved for the emittance using Equation (1). Finally, one gets the spectral directional emittance $\varepsilon_{\mathrm{d},\lambda}$ at the sample temperature T_{sp}:

$$\varepsilon_{\mathrm{d},\lambda}(T_{\mathrm{sp}}) = \frac{i_{\lambda,\mathrm{meas}}(T_{\mathrm{sp}},T_{\mathrm{b}}) - i_{\lambda,\mathrm{bb}}(T_{\mathrm{b}})}{i_{\lambda,\mathrm{bb}}(T_{\mathrm{sp}}) - i_{\lambda,\mathrm{bb}}(T_{\mathrm{b}})} \quad . \tag{4}$$

Hence, the spectral directional emittance $\varepsilon_{\mathrm{d},\lambda}$ can be determined at high temperatures from the measured spectral intensity $i_{\lambda,\mathrm{meas}}(T_{\mathrm{sp}},T_{\mathrm{b}})$ together with the calculated spectral intensity of a black body at the sample temperature $i_{\lambda,\mathrm{bb}}(T_{\mathrm{sp}})$ and the temperature of the black enclosure $i_{\lambda,\mathrm{bb}}(T_{\mathrm{b}})$.

The configuration of Figure 4 (d) corresponds with that of Figure 4 (a), but the temperature T_{a} of the black enclosures is lower, which leads to a similar formula for the spectral directional emittance $\varepsilon_{\mathrm{d},\lambda}$ with the temperature T_{a} instead of the temperature T_{b}.

With the configurations in Figure 4 (b) and Figure 4 (c) it is possible to measure the spectral directional-hemispherical reflectance $R_{\mathrm{dh},\lambda}$ and transmittance $T_{\mathrm{dh},\lambda}$, respectively. Together with the configuration shown in Figure 4 (a) or Figure 4 (d) three measurements can be performed in order to determine the spectral emittance, reflectance and transmittance. Thus, the directional-hemispherical transmittance $T_{\mathrm{dh},\lambda}$ can be derived as function of two measured spectra and two calculated Planckian spectra $i_{\lambda,\mathrm{bb}}$ at the temperatures T_b and T_a:

$$T_{\mathrm{dh},\lambda}(T_\mathrm{sp}) = \frac{i_{\lambda,\mathrm{meas}}(T_\mathrm{sp},T_\mathrm{b}) - i_{\lambda,\mathrm{meas}}(T_\mathrm{sp},T_\mathrm{b},T_\mathrm{a})}{i_{\lambda,\mathrm{bb}}(T_\mathrm{b}) - i_{\lambda,\mathrm{bb}}(T_\mathrm{a})} \quad . \tag{5}$$

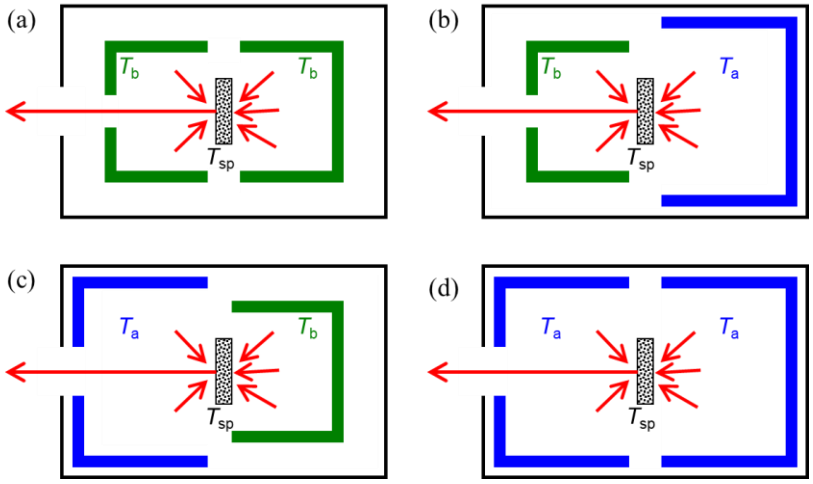

Figure 4. Different measurement setups of the black body boundary conditions (BBC) apparatus for determining the infrared-optical properties of a sample at the temperature T_sp.

The derived transmittance $T_{\mathrm{dh},\lambda}$ at ambient and high temperatures can be found in Figure 5 for sapphire, which consists of highly dense Al_2O_3 without porosity. Sapphire exhibits a high transmittance for wavelengths up to 6 µm at ambient temperature and 5 µm at temperatures around 1200 K. For wavelengths above 7 µm the transmittance vanishes and the emittance increases significantly. Furthermore, for wavelengths below 4 µm the transmittance only slightly depends on temperature.

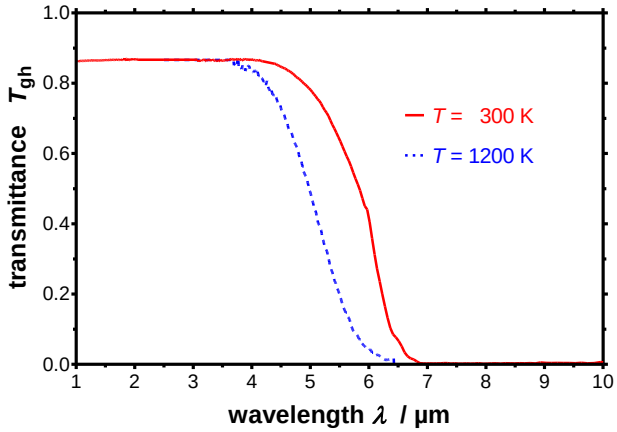

Figure 5. Directional-hemispherical transmittance $T_{\mathrm{dh},\lambda}$ of sapphire with a thickness of d = 1 mm measured at different temperatures T, versus wavelength from 1 µm to 10 µm.

NON-CONTACT DETERMINATION OF THE ADHESIVE PROPERTIES

For investigating the adhesive properties of ceramic coatings a contactless measurement procedure has been developed, which enables a non-destructive detection of delamination or debonding, which uses the derived infrared-optical properties of the applied materials as input parameters.

First, a simplified experiment has been performed in order to validate the temperature measurements of the substrate and the coating using radiation thermometers (pyrometers), which are sensitive at different wavelength regions. For performing these measurements, a sapphire sample has been placed directly onto a metallic substrate and with a gap above the substrate as illustrated in Figure 6. Sapphire has been chosen due to its high transmittance in the near infrared (NIR) and its high emittance in the long-wavelength infrared (LWIR) as describe above. The measurements have been performed with two radiation thermometers, which are sensitive at 1 µm (NIR-pyrometer) and 10 µm (LWIR-pyrometer), respectively. At a wavelength of 1 µm mainly radiation from the substrate is detected by the NIR-pyrometer whereas at a wavelength of 10 µm only radiation from the sapphire surface is detected by the LWIR-pyrometer. The substrate has been heated up to a temperature of 900 K and 1500 K and the temperatures of the metallic substrate and the sapphire surface have been determined using the NIR- und LWIR-pyrometer. The detected temperatures of the sapphire surfaces for the two cases (without and with gap) are shown in Figure 7. The temperature of the sapphire sample without gap is significantly higher than the temperature of the sapphire sample with gap as the gap increases the thermal contact resistance.

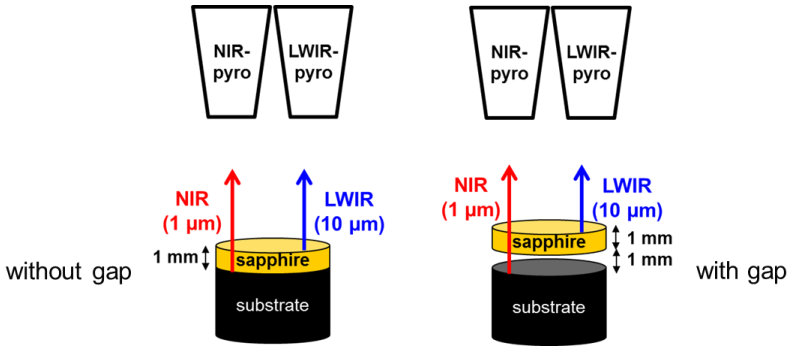

Figure 6. Test setup for determining the influence of a gap onto the temperature gradient by performing non-contact temperature measurements using radiation thermometers (pyrometers), which are sensitive at two difference wavelengths, 1 µm (NIR) and 10 µm (LWIR).

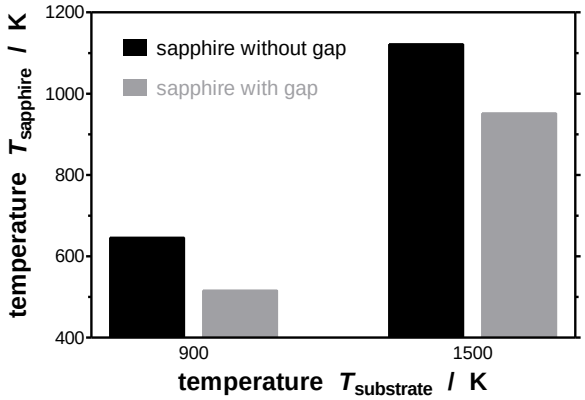

Figure 7. Detected temperatures with the long wavelength radiation thermometer of the sapphire surface versus the temperature of the substrate for two cases: sapphire without gap and sapphire with gap.

Finally, a novel non-destructive and contactless method for quantifying thermal and mechanical adhesion of layers has been developed, which will be described in the following. The surface of the coated sample or layered system is heated by a laser pulse, which is guided by an optical waveguide onto the surface. By varying pulse time, position and diameter of the laser beam the energy density irradiated onto the surface can be controlled. The resulting temperature profile is measured by a thermographic camera (Infratec VarioCAM®) as shown in Figure 8. The procedure is also known as active thermography [Hung et al. (2009)]. For this purpose, the setup depicted in Figure 8 consists of two main components:

- a laser with an optical fibre and rotatable optics, which serves as energy source for inserting heat into the coating and
- a thermographic camera, which measures the lateral temperature distribution across the surface of the coating.

The surface temperature of the coating locally increases at positions where an increased thermal contact resistance occurs. As an increased thermal contact resistance is usually correlated with a partial delamination of the TBC, this method is suitable to detect partial delaminations, especially if they are not yet optically perceivable.

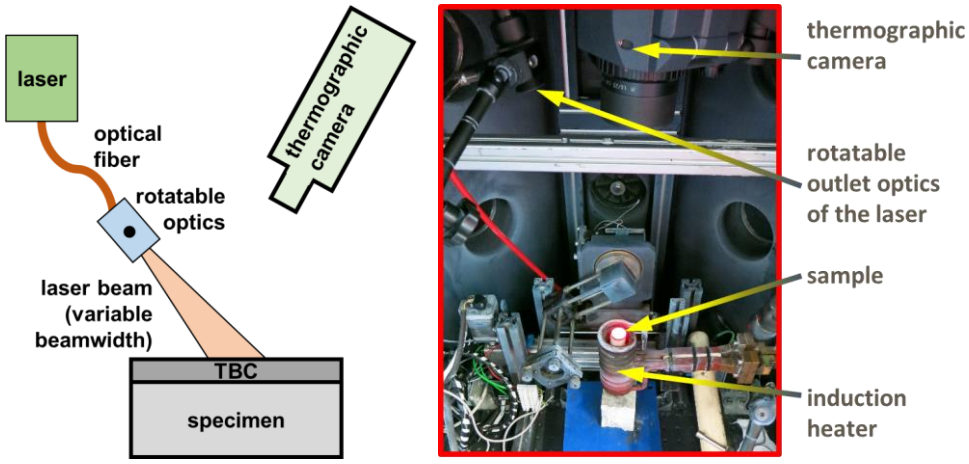

Figure 8. Scheme of the non-destructive and contactless method for measuring layer systems with active thermography using a laser and a thermographic camera (depicted on the left) and photo of the setup (shown on the right).

For testing the developed setup, samples have been prepared by Rauschert Heinersdorf-Pressig GmbH (Bahnhofstraße 1, 96332 Pressig, Germany) with a defined partial delamination by applying a coating by atmospheric plasma spraying (APS) on a metal substrate with a thickness of 2 mm. The coating with a thickness of 200 µm consists of Al_2O_3 (97 wt-%) and TiO_2 (3 wt-%). For creating an air gap with a certain geometry (e.g. a line as shown in Figure 9 top left) between the substrate and the coating, at first a bond coat (NiCrAlY-alloy) with a thickness of 30 µm was only applied onto the grey areas of the discoidal substrate in Figure 9 (top left) leaving the white area uncoated. Afterwards the top-coat was applied onto the whole area of the substrate. Finally, the sample, which consists of substrate, partial bond coat and top-coat, was annealed at 800 °C for 2 h. Because of the annealing, an air gap occurred between the substrate and the top-coat in the areas without bond coat. This is due to the fact, that the adhesion of the top-coat to the bond coat is strong, whereas the adhesion of the top-coat to the substrate is weak.

Beside this partial delamination, the top-coat is intact and no damage is visible when looking at the top-coat. Hence, on a photograph of the surface (Figure 9 top right) no delamination can be seen. However, the partial delamination can be detected and visualized by performing the non-destructive test, which is

described above. A collection of selected thermographic images, which have been generated during the heating and the cooling period, is shown at the bottom of Figure 9. On the first picture, no structure is visible as all surfaces exhibit the same temperature. After turning the laser on, the surface temperature increases. The temperature rise is significantly higher at the position of the air gap, compared to the temperature rise at other positions without air gap. As previously explained the heat load is efficiently dissipated onto the substrate if a strong adhesion exists. However, the air gap reduces the heat flow onto the substrate and thus the dissipation of the heat input, which leads to a locally higher surface temperature at the position of the air gap. After turning the laser off, the surface temperature decreases and finally the differences in temperature disappear, whereat the surface temperature at the end is slightly higher than at the beginning.

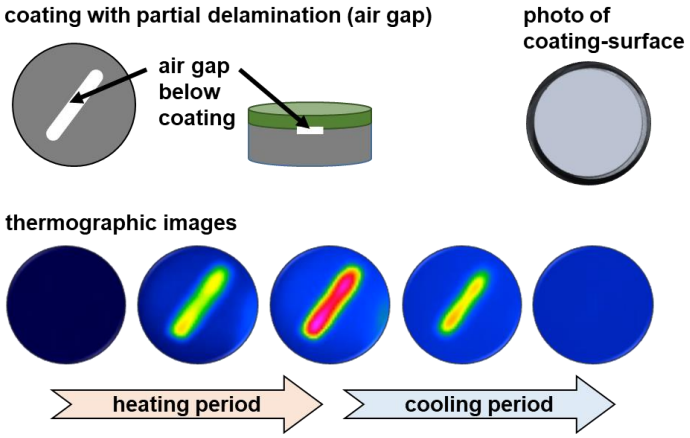

Figure 9. Coating on a metal substrate with defined partial delamination (top left) and temperature distributions on the coating surface determined by active thermography during the heating and cooling phase (bottom). No delamination is visible on a photo of the coating surface (top right).

Furthermore, it is possible to heat up the investigated samples to high temperatures using an inductive heating device. With a laser pulse, which generates an additional temperature rise it is possible to detect delaminations at high temperatures, too. An example for a coating with another linear flaw is presented in Figure 10. The flaw below the coating is not visible in the top view (left of Figure 10). On the right side of Figure 10 a thermal image is shown, which has been taken during the cooling phase after a laser pulse has heated up the surface of the coating. The linear flaw is clearly visible on the thermal image due to the locally increased temperature profile.

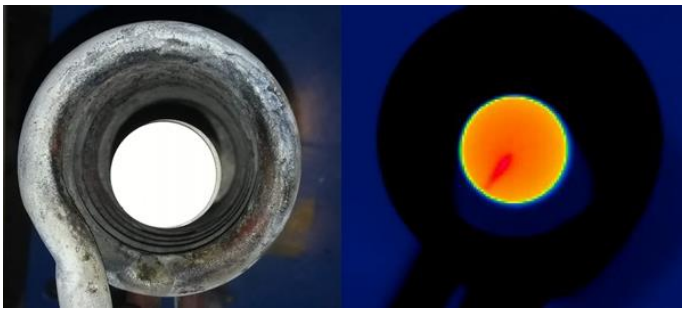

Figure 10. Photo of a disc-shaped steel specimen with a ceramic coating on top placed in an inductive heating device (on the left) and thermal image of the specimen after heating by an additional laser pulse (on the right). A partial delamination (linear flaw) of the coating is clearly visible on the thermal image, although it is not visible on the photo.

These investigations can also be performed on large samples (see Figure 11). For this purpose, again a coating with defined delamination has been prepared on a metallic substrate. A photo of the surface is given on the left in Figure 11. On this photo no delamination or defect can be identified. In contrast to that a circular delamination can be detected by a thermographic camera as displayed in the thermogram on the right in Figure 11. Another sample with visible flaking and non-visible delamination is depicted on the left in Figure 12. On the thermogram besides the flaking a crosswise delamination has been detected as depicted on the right in Figure 12.

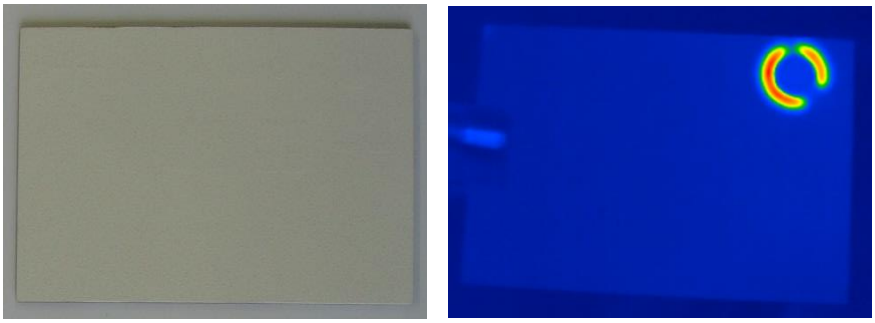

Figure 11. Photo of TBC surface (left) and thermal image of a TBC surface after laser heating (right), where the circular delamination of the coating is clearly visible.

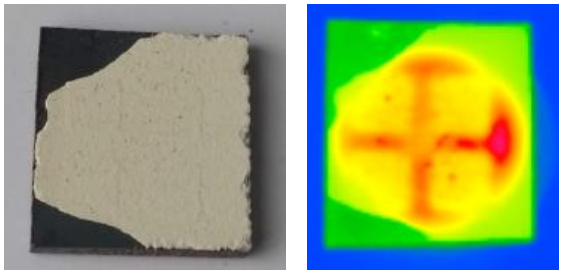

Figure 12. Photo of TBC surface (left) and thermal image of the TBC surface after laser heating (right). On the photo flaking in 2 edges is clearly visible, but no further defects are perceivable. In the thermal image the flaking in 2 edges can be seen, too. Additionally, a crosswise delamination is observable.

CONCLUSION

A non-destructive and contactless measurement method for detecting the adhesive properties of ceramic coatings has been successfully developed and validated. As the method relies on optical properties of the investigated materials, at first measurements of the optical properties of the samples, i.e. reflectivity, transmissivity and finally emissivity have been performed. Finally, for detecting the adhesive properties of ceramic coatings, the local distribution of the surface temperatures of the coating after irradiating with a laser for a defined time period has been measured using a thermographic camera. This procedure allows the determination of local delaminations of coatings, although these delaminations are not visible. Tests of the measurement procedure have been performed on tailor-made samples with well-defined local delaminations. These prepared delaminations could have been detected by the developed method, although these delaminations were not visible by visual inspection as the coatings were intact with the only exception of these delaminations.

Based on the investigations in the laboratory, the method can be scaled up for application in industrial environments for contactless and non-destructive examination (NDE) during operation or maintenance as

well as during or after the coating process. With the developed method, it is possible to detect local delaminations prior to a large-area debonding and a complete failure of the coating. Hence, a new technique is available for testing the structural integrity of layer systems, which can be adapted to specific applications.

ACKNOWLEDGMENT

This research was funded by EMPIR program co-financed by the Participating States and from the European Union's Horizon 2020 research and innovation program (grant number: 17IND11-Hi-TRACE) and by the Federal Ministry for Economic Affairs and Climate Action (BMWK) on the basis of a decision by the German Bundestag (grant number: 03ET7082A).

REFERENCES

Ahrens, M., Lampenscherf, S., Vaßen, R. and Stöver, D. (2004). "Sintering and creep processes in plasma-sprayed thermal barrier coatings," *Journal of Thermal Spray Technology*, 13 (3) 432–442

Choi, S. R., Hutchinson, J. W., and Evans A. G. (1999). "Delamination of multilayer thermal barrier coatings," *Mechanics of Materials*, 31 431-447

Eldridge, J. I., Spuckler, C. M. and Martin R. E. (2006). "Monitoring Delamination Progression in Thermal Barrier Coatings by Mid-Infrared Reflectance Imaging," *Int. J. Appl. Ceram. Technol.*, 3 (2) 94-104

Evans, A. G., Mumm, D. R., Hutchinson, J. W., Meier, G. H. and Pettit, F. S. (2001). "Mechanism controlling the durability of thermal barrier coatings," *Progress in Material Science*, 46 505-553

Hanssen, L. (2001). "Integrating-sphere system and method for absolute measurement of transmittance, reflectance, and absorptance of specular samples," *Applied Optics*, 40 3196-3204

Hung, Y. Y., Chen, Y. S., Ng, S. P., Liu, L. Huang, Y. H., Luk, B. L., Ip, R. W. L., Wu, C. M. L., Chung, P. S. (2009). "Review and comparison of shearography and active thermography for nondestructive evaluation," *Materials Science and Engineering: R: Reports*, 64 (5-6) 73-112

Hutchinson, J. W, and Evans A. G. (2002). "On the delamination of thermal barrier coatings in a thermal gradient," *Surface and Coatings Technology*, 149 179-184

Ito, K., Kuriki, H., Araki, H., Kuroda, S. and Enoki M. (2014) "Detection of segmentation cracks in top coat of thermal barrier coatings during plasma spraying by non-contact acoustic emission method," *Sci. Technol. Adv. Mater.*, 15 035007

Li, Y., Chen, Z., Maoa, Y. and Qi, Y. (2012). "Quantitative evaluation of thermal barrier coating based on eddy current technique," *NDT&E International*, 50 29-35

Manara, J., Caps, R., Ebert, H.-P., Hemberger, F., Fricke, J. and Seidl, A. (2001) "Infrared optical properties of semitransparent pyrolytic boron nitride (pBN)," *High Temp. – High Press.*, 34 65–72

Manara, J., Arduini-Schuster, M., and Hanssen L. (2009a). "Infrared-optical intercomparison measurements for evaluating the accuracies of the achieved results," *High Temp. – High Press.*, 38 259-276

Manara, J., Arduini-Schuster, M., Rätzer-Scheibe, H.-J. and Schulz U. (2009b). "Infrared-optical properties and heat transfer coefficients of semitransparent thermal barrier coatings," *Surf. Coat. Technol.*, 203 1059-1068

Nitin, P. P., Maurice, G. und Eric, H. J. (2002). "Thermal Barrier Coatings for Gas-Turbine Engine Applications," *Science*, 296 280-284

Tolpygo, V. K., Clarke, D. R. and Murphy, K. S. (2004). "Evaluation of interface degradation during cyclic oxidation of EB-PVDthermal barrier coatings and correlation with TGO luminescence," *Surface & Coatings Technology*, 188–189 62-70

Zhang, H., Liu, Z., Yang, X. and Xie, H. (2019). "Interface failure behavior of YSZ thermal barrier coatings during thermal shock," *Journal of Alloys and Compounds*, 779 686-697